BULLETIN OF THE POLISH ACADEMY OF SCIENCES
TECHNICAL SCIENCES, Vol. 67, No. 6, 2019
DOI: 10.24425/bpasts.2019.130888

Engineering design of low-head Kaplan hydraulic turbine blades using the inverse problem method

Z. KRZEMIANOWSKI*

The Szewalski Institute of Fluid-Flow Machinery of the Polish Academy of Sciences, J. Fiszera 14, 80-231 Gdańsk, Poland

Abstract. The paper concerns the engineering design of guide vane and runner blades of hydraulic turbines using the inverse problem on the basis of the definition of a velocity hodograph, which is based on Wu's theory [1, 2]. The design concerns the low-head double-regulated axial Kaplan turbine model characterized by a very high specific speed. The three-dimensional surfaces of turbine blades are based on meridional geometry that is determined in advance and, additionally, the distribution of streamlines must also be defined. The principles of the method applied for the hydraulic turbine and related to its conservation equations are also presented. The conservation equations are written in a curvilinear coordinate system, which adjusts to streamlines by means of the Christoffel symbols. This leads to significant simplification of the computations and generates fast results of three-dimensional blade surfaces. Then, the solution can be found using the method of characteristics. To assess usefulness of the design and robustness of the method, numerical and experimental investigations in a wide range of operations were carried out. Afterwards, the so-called shell characteristics were determined by means of experiments, which allowed to evaluate the method for application to the low-head (1.5 m) Kaplan hydraulic turbine model with the kinematic specific speed (∼260). The numerical and experimental results show the successful usage of the method and it can be concluded that it will be useful in designing other types of Kaplan and Francis turbine blades with different specific speeds.

Key words: inverse method, hydraulic turbine blade design, low-head Kaplan turbine, curvilinear coordinate system, Christoffel symbols.

1. Introduction

The design of rotating machines including hydraulic turbines and pumps is difficult and requires a comprehensive approach in order to achieve high efficiency and avoid the cavitation phenomenon. This is due to the phenomena occurring in flow passage, which are described by non-linear equations that have to be solved to obtain the flow field. The use of iterative way of designing by means of CFD methods now significantly improves this process and allows for peer numerical analysis of phenomena such as: secondary flows, cavitation prediction, etc. However, on the other hand, the use of CFD is often related to the time-consuming process of determining blade geometry (often, the design of such geometry must be relatively quick for a customer) because direct design (problem) introduces the difficulty of determining the direction of changes leading to the improvement of the blade design due to the complicated three-dimensional nature of the flow through the machine. Then, as an alternative, the inverse problem blade design (determination of the skeleton blade surface) may be helpful, which is significantly faster than the blade design using the direct problem. Obviously, it constitutes good practice to use CFD analysis because the inverse problem design provides the blade geometry at one point of operation, which is supposed to be the best efficiency point (BEP). In fact, it may happen that it works well at this point but the efficiency may rapidly decrease in its vicinity (i.e. by changing the flow rate or/and head). In such cases, CFD is a very powerful tool to evaluate off-design machine operation. Additionally, it helps eliminate significant mistakes in the design process.

Over the years, a number of activities in the application of the inverse problem to turbomachinery have been performed, caused *inter alia* by the significant development of computers. A vast amount of research regarding the issue of the design process for turbomachines with incompressible and compressible flows was published in the past 4 decades. The improvements proposed through the years for turbomachinery (gas turbines, compressors, pumps) by as part of inverse design introduced extensive development and progress of its performance [3–8]. Relating to hydraulic machines, in many papers researchers presented the advantages of two-dimensional and a three-dimensional inverse problem applications to pumps and hydraulic turbines and their operational optimization [9–14]. An approach to the optimization of losses and cavitation number in the axial flow turbine runner can also be found in papers [15, 16]. The common availability of the CFD commercial codes provided for the possibility of an interactive aided inverse design process of hydraulic machines. It still remains faster and less time-consuming than designing by means of analyzing with the use of the CFD alone. For instance, interaction with the CFD allows for eliminating/reducing the secondary flows [17, 18] or reducing the area of pressure below the vapor pressure, which means decreasing intensity of the cavitation phenomenon [19] and/or estimating the hydrodynamic and suction performance [20]. Generally, mutual interaction of the inverse problem and CFD calculations leads to improving operational parameters, especially the efficiency of hydraulic machines and anti-cavitation performance. However, in some cases in which a fast technical design is required, particularly in the case of small low-cost low-head hydraulic turbines, CFD

*e-mail: krzemian@imp.gda.pl

Manuscript submitted 2019-01-25, revised 2019-03-26, initially accepted for publication 2019-04-19, published in December 2019

cannot be used because of too long time required. In such cases design by means of an inverse problem is indispensable.

Generally, inverse problems in hydrodynamics are based on potential flow models [21–24] or the flow models using Euler's equation [7, 25], in which slip condition is imposed at the walls. Models containing viscosity (non-slip condition), i.e. using the Navier-Stokes equation [8, 26], can already be encountered.

The goal of the current work is to design a blade cascade (double-adjustable turbine) by means of the inverse problem method using hodograph theory. The principles of theory are derived from the fundamental works of Wu [1, 2], which are based on the concept of two surfaces called *S*1 (streamline surfaces) and *S*2 (blade surfaces). Generally, this inverse method is suitable for a wide range of subtypes of turbomachines. The basics of this method in application to the design of the Kaplan hydraulic turbine guide vane and runner blades with the very high kinematic specific speed $n_{sq} = \sim 260$ are presented. This quantity is extremely important for the engineering design process of hydraulic turbines because it determines their meridional shape and is defined as follows (note: this is not a non-dimensional quantity):

$$n_{sq} = \frac{n\,Q^{0.5}}{H^{0.75}} \tag{1}$$

where n is the rotational speed [rpm], Q is the volumetric flow rate $\left[\mathrm{m}^3/\mathrm{s}\right]$ and H is the head [m].

2. Theoretical background

2.1. The principles. The flow through the rotating machine is fully three-dimensional due to the phenomena occurring in the flow (secondary flows, blade vortices, pressure pulsations on the blades and in the draft tube). However, with well-posed boundary conditions, in the case of hydraulic machinery such as hydraulic turbines (particularly low-head ones), fast engineering methods containing significant simplifications may be considered to be sufficient for engineering purposes to achieve good results of the design.

In order to significantly simplify the solution to the inverse problem, it is convenient to write the set of conservation equations in a curvilinear system by introducing curvilinear coordinates $x^{(1)}, x^{(2)}, x^{(3)}$. The first of them is constant along each streamline [–] and it varies (in a spanwise direction) within the range of 0 (at hub) to 1 (at shroud). The second one is the angular coordinate [rad] and the third one is the axial coordinate [m] – Fig. 1.

The flow is considered to act on the streamlines that are related to streamline function denoted as f. This is a radius perpendicular to rotational axis $\left(\text{depends on two coordinates } x^{(1)}, x^{(3)}\right)$, which has to be specified in advance, and can be written as follows:

$$f\left(x^{(1)}, x^{(3)}\right) = f. \tag{2}$$

Transformation to the new coordinate system requires assuming the transition rules between the Cartesian (x, y, z) and the newly introduced curvilinear system. If cylindrical transition is assumed, then using the definition of hodograph $\vec{r}$, the following relationship can be written:

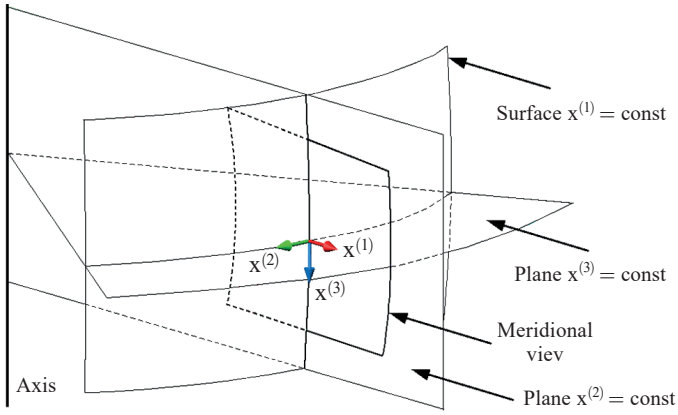

Fig. 1. Schematic of the curvilinear coordinate system

$$\begin{aligned}\vec{\mathbf{r}} &= x\,\vec{\mathbf{i}} + y\,\vec{\mathbf{j}} + z\,\vec{\mathbf{k}} = \\ &= f\cos\left(x^{(2)}\right)\vec{\mathbf{i}} + f\sin\left(x^{(2)}\right)\vec{\mathbf{j}} + x^{(3)}\vec{\mathbf{k}}\end{aligned} \tag{3}$$

where $\vec{i}$, $\vec{j}$, $\vec{k}$ are the unit vectors of the Cartesian coordinate system.

In the new coordinate system, the hodograph will be written as follows:

$$\vec{\mathbf{r}} = x^{(i)}\,\vec{\mathbf{e}}_{\mathbf{i}} = x^{(1)}\,\vec{\mathbf{e}}_{\mathbf{1}} + x^{(2)}\,\vec{\mathbf{e}}_{\mathbf{2}} + x^{(3)}\,\vec{\mathbf{e}}_{\mathbf{3}}\,. \tag{4}$$

The quantity $\vec{e}_i$ is the contravariant vector of the new coordinate system as follows:

$$\vec{\mathbf{e}}_{\mathbf{i}} = \frac{\partial \vec{\mathbf{r}}}{\partial x^{(i)}} \quad \text{where } i = 1, 2, 3. \tag{5}$$

Using this, the covariant basis of the new coordinate system can also be defined as follows:

$$\vec{\mathbf{e}}^{\mathbf{i}} = \frac{\vec{\mathbf{e}}_{\mathbf{j}} \times \vec{\mathbf{e}}_{\mathbf{k}}}{\vec{\mathbf{e}}_{\mathbf{1}} \circ (\vec{\mathbf{e}}_{\mathbf{2}} \times \vec{\mathbf{e}}_{\mathbf{3}})} \quad \text{where } i, j, k = 1, 2, 3. \tag{6}$$

The contravariant metric tensor of three-dimensional space $\tilde{g}_{ij}$ is given by the following:

$$\begin{aligned}\tilde{g}_{ij} &= \begin{vmatrix} \vec{\mathbf{e}}_{\mathbf{1}} \circ \vec{\mathbf{e}}_{\mathbf{1}} & \vec{\mathbf{e}}_{\mathbf{1}} \circ \vec{\mathbf{e}}_{\mathbf{2}} & \vec{\mathbf{e}}_{\mathbf{1}} \circ \vec{\mathbf{e}}_{\mathbf{3}} \\ \vec{\mathbf{e}}_{\mathbf{2}} \circ \vec{\mathbf{e}}_{\mathbf{1}} & \vec{\mathbf{e}}_{\mathbf{2}} \circ \vec{\mathbf{e}}_{\mathbf{2}} & \vec{\mathbf{e}}_{\mathbf{2}} \circ \vec{\mathbf{e}}_{\mathbf{3}} \\ \vec{\mathbf{e}}_{\mathbf{3}} \circ \vec{\mathbf{e}}_{\mathbf{1}} & \vec{\mathbf{e}}_{\mathbf{3}} \circ \vec{\mathbf{e}}_{\mathbf{2}} & \vec{\mathbf{e}}_{\mathbf{3}} \circ \vec{\mathbf{e}}_{\mathbf{3}} \end{vmatrix} = \\ &= \begin{vmatrix} \left(\frac{\partial f}{\partial x^{(1)}}\right)^2 & 0 & \frac{\partial f}{\partial x^{(1)}}\frac{\partial f}{\partial x^{(3)}} \\ 0 & f^2 & 0 \\ \frac{\partial f}{\partial x^{(1)}}\frac{\partial f}{\partial x^{(3)}} & 0 & 1 + \left(\frac{\partial f}{\partial x^{(3)}}\right)^2 \end{vmatrix}\end{aligned} \tag{7}$$

and, similarly, the covariant metric tensor of three-dimensional space $\tilde{g}^{ij}$ is given as:

$$\tilde{g}^{ij} = \begin{vmatrix} \vec{\mathbf{e}}^{\mathbf{1}} \circ \vec{\mathbf{e}}^{\mathbf{1}} & \vec{\mathbf{e}}^{\mathbf{1}} \circ \vec{\mathbf{e}}^{\mathbf{2}} & \vec{\mathbf{e}}^{\mathbf{1}} \circ \vec{\mathbf{e}}^{\mathbf{3}} \\ \vec{\mathbf{e}}^{\mathbf{2}} \circ \vec{\mathbf{e}}^{\mathbf{1}} & \vec{\mathbf{e}}^{\mathbf{2}} \circ \vec{\mathbf{e}}^{\mathbf{2}} & \vec{\mathbf{e}}^{\mathbf{2}} \circ \vec{\mathbf{e}}^{\mathbf{3}} \\ \vec{\mathbf{e}}^{\mathbf{3}} \circ \vec{\mathbf{e}}^{\mathbf{1}} & \vec{\mathbf{e}}^{\mathbf{3}} \circ \vec{\mathbf{e}}^{\mathbf{2}} & \vec{\mathbf{e}}^{\mathbf{3}} \circ \vec{\mathbf{e}}^{\mathbf{3}} \end{vmatrix} =$$

$$= \begin{vmatrix} \frac{1+\left(\frac{\partial f}{\partial x^{(3)}}\right)^2}{\left(\frac{\partial f}{\partial x^{(1)}}\right)^2} & 0 & -\frac{\frac{\partial f}{\partial x^{(3)}}}{\frac{\partial f}{\partial x^{(1)}}} \\ 0 & \frac{1}{f^2} & 0 \\ -\frac{\frac{\partial f}{\partial x^{(3)}}}{\frac{\partial f}{\partial x^{(1)}}} & 0 & 1 \end{vmatrix}. \tag{8}$$

The velocity field may be written in the following form:

$$\vec{\mathbf{U}} = U^{(i)}\vec{\mathbf{e}}_{\mathbf{i}} = U_{(i)}\vec{\mathbf{e}}^{\mathbf{i}} = U_{x^{(i)}}\vec{\mathbf{l}}_{\mathbf{i}} \tag{9}$$

where $U^{(i)}$ are the contravariant components of the velocity vector, $U_{(i)}$ are the covariant components of the velocity vector and $U_{x^{(i)}}$ are the physical components of the velocity vector related to physical base $\vec{l}_i$.

In the further part of the paper, only the contravariant and physical components of the velocity vector will be used. The relationship between the contravariant and physical bases is as follows:

$$U_{x^{(i)}} = U^{(i)}\sqrt{\tilde{g}_{ii}}\,. \tag{10}$$

Therefore, the velocity components will be, respectively:

$$U_{x^{(1)}} = U^{(1)}\sqrt{\tilde{g}_{11}} = U^{(1)}\left|\frac{\partial f}{\partial x^{(1)}}\right| \equiv 0 \tag{11}$$

$$U_{x^{(2)}} = U^{(2)}\sqrt{\tilde{g}_{22}} = U^{(2)}|f| = U^{(2)}f \neq 0 \tag{12}$$

$$U_{x^{(3)}} = U^{(3)}\sqrt{\tilde{g}_{33}} = U^{(3)}\sqrt{1+\left(\frac{\partial f}{\partial x^{(3)}}\right)^2} \neq 0. \tag{13}$$

The $U^{(1)}$ component (and, respectively, $U_{x^{(1)}}$ as well) is identically equal to zero because it is related to the $x^{(1)}$ coordinate (the velocity vector is tangent to a streamline). The other velocities mean the following: $U^{(2)}$ is the angular velocity, $U_{x^{(2)}}$ is the tangential velocity, $U^{(3)}$ is the axial velocity and $U_{x^{(3)}}$ is the meridional velocity (resultant velocity of axial and radial velocities).

Let us introduce the so-called Christoffel symbols of the second kind [27, 28], denoted as $\Gamma^k_{i,j}$, that allow for transforming the conservation equations from the Cartesian to the new coordinate system. They can be obtained after carrying out the following scalar multiplication:

$$\vec{\mathbf{e}}^{\mathbf{k}} \circ d\vec{\mathbf{e}}_{\mathbf{j}} = \vec{\mathbf{e}}^{\mathbf{k}} \circ d\left(\frac{\partial \vec{\mathbf{r}}}{\partial x^{(j)}}\right) = \underbrace{\vec{\mathbf{e}}^{\mathbf{k}} \circ \frac{\partial^2 \vec{\mathbf{r}}}{\partial x^{(j)}\partial x^{(i)}}}_{\Gamma^k_{i,j}} dx^{(i)} = \tag{14}$$

$$= \Gamma^k_{i,j}\, dx^{(i)}.$$

The individual values of the Christoffel symbols form a three-dimensional matrix with 27 components ($3\times3\times3 = 27$) and take the form shown in the Appendix.

The formula for the differentiation of velocity related to contravariant coordinates is:

$$\frac{(dU)^k}{dx^{(i)}} = \frac{\partial U^{(k)}}{\partial x^{(i)}} + \Gamma^k_{i,j}U^{(j)} = \nabla_i U^{(k)} \quad \text{where } \nabla_i = \frac{\partial}{\partial x^{(i)}}. \tag{15}$$

If $i = k$, then the formula for the divergence of velocity is obtained:

$$\nabla_i U^{(i)} = \frac{\partial U^{(i)}}{\partial x^{(i)}} + \Gamma^i_{i,j}U^{(j)}. \tag{16}$$

Hence, in the presented case, it can be written as follows:

$$\mathbf{div}\vec{\mathbf{U}} = \frac{\partial U^{(3)}}{\partial x^{(3)}} + \Gamma^1_{1,3}U^{(3)} + \Gamma^2_{2,3}U^{(3)}. \tag{17}$$

The gradient of any scalar function S in a curvilinear system is as follows:

$$\vec{\mathbf{s}} = \mathbf{grad}\, S = \boldsymbol{\nabla}_{\mathbf{i}}\,\vec{\mathbf{e}}_{\mathbf{i}}\, S = s^{(i)}\,\vec{\mathbf{e}}_{\mathbf{i}} = s_{(i)}\,\vec{\mathbf{e}}^{\mathbf{i}} \tag{18}$$

in which:

$$s^{(i)} = s_{(j)}\,\tilde{g}^{ji} \tag{19}$$

and in which:

$$s_{(j)} = \frac{\partial}{\partial x^{(j)}}S. \tag{20}$$

The substantial derivative of velocity will be:

$$\frac{\partial \vec{\mathbf{U}}}{\partial t} + \vec{\mathbf{U}} \circ \mathbf{grad}\,\vec{\mathbf{U}} = \frac{\partial U^{(k)}}{\partial t}\vec{\mathbf{e}}_{\mathbf{k}} + U^{(i)}\,\nabla_i\, U^{(k)}\,\vec{\mathbf{e}}_{\mathbf{k}} = \tag{21}$$

$$= U^{(i)}\left(\frac{\partial U^{(k)}}{\partial x^{(i)}} + \Gamma^k_{i,j}U^{(j)}\right)\vec{\mathbf{e}}_{\mathbf{k}}\,.$$

Therefore, the components of the velocity gradient for the presented model in a curvilinear system will be as follows:

$$s^{(1)} = U^{(2)}\left(\Gamma^1_{2,2}\,U^{(2)}\right) + U^{(3)}\left(\Gamma^1_{3,3}\,U^{(3)}\right) \tag{22}$$

$$s^{(2)} = U^{(3)}\frac{\partial U^{(2)}}{\partial x^{(3)}} + U^{(2)}\left(\Gamma^2_{2,3}U^{(3)}\right) + \tag{23}$$

$$+ U^{(3)}\left(\Gamma^2_{3,2}U^{(2)}\right)$$

$$s^{(3)} = U^{(3)}\frac{\partial U^3}{\partial x^{(3)}}\,. \tag{24}$$

It should be emphasized that the components of the physical base, used in the conservation equations, are then similarly recalculated, as presented in formula (10):

$$s_{x^{(i)}} = s^{(i)}\sqrt{\tilde{g}_{ii}}\,. \tag{25}$$

Now, in the further part of the paper, it is already possible to form the conservation equations in a curvilinear coordinate system.

2.2. Mass conservation equation. The mass conservation equation (MassCE) using (16) and (17) will take the following form:

$$\rho\,\mathbf{div}\vec{\mathbf{U}} = \rho\left(\frac{\partial U^{(3)}}{\partial x^{(3)}} + U^{(3)}\left(\frac{\frac{\partial^2 f}{\partial x^{(3)}\partial x^{(1)}}}{\frac{\partial f}{\partial x^{(1)}}} + \frac{\frac{\partial f}{\partial x^{(3)}}}{f}\right)\right) = 0 \quad (26)$$

where ρ is the density.

It can be proven that the expression in the internal parenthesis may be written as follows:

$$U^{(3)}\left(\frac{\frac{\partial^2 f}{\partial x^{(3)}\partial x^{(1)}}}{\frac{\partial f}{\partial x^{(1)}}} + \frac{\frac{\partial f}{\partial x^{(3)}}}{f}\right) \equiv \frac{U^{(3)}}{2\,det[\tilde{g}_{ij}]}\frac{\partial(det[\tilde{g}_{ij}])}{\partial x^{(3)}} \quad (27)$$

where $det[\tilde{g}_{ij}]$ is the determinant of the contravariant tensor given by equation (7), having the following form:

$$det[\tilde{g}_{ij}] = \left(f\,\frac{\partial f}{\partial x^{(1)}}\right)^2. \quad (28)$$

Thus, after some algebraic transformations, MassCE will take the following form:

$$\frac{1}{\sqrt{det[\tilde{g}_{ij}]}}\frac{\partial}{\partial x^{(3)}}\left(\rho\,U^{(3)}\sqrt{det[\tilde{g}_{ij}]}\right) = 0 \quad (29)$$

and after integration it will be:

$$\rho\,U^{(3)}\sqrt{det[\tilde{g}_{ij}]} = m\left(x^{(1)}\right) \quad (30)$$

where $m\left(x^{(1)}\right)$ is the mass flow at the inlet to the blade channel (boundary condition for the MassCE).

Finally, MassCE, including (13), will be:

$$\frac{(1-\vartheta)\,\rho\,U_{x^{(3)}}\,f\left|\frac{\partial f}{\partial x^{(1)}}\right|}{\sqrt{1+\left(\frac{\partial f}{\partial x^{(3)}}\right)^2}} = m\left(x^{(1)}\right) \quad (31)$$

where $\vartheta = \vartheta\left(x^{(1)}, x^{(3)}\right)$ is the non-dimensional blockage factor taking the non-zero blade thickness into account.

2.3. Momentum conservation equation. In the presented model, the momentum conservation equation (MomCE) is Euler's equation:

$$\rho\,\frac{d\vec{\mathbf{U}}}{dt} = -\rho\,\mathbf{grad}\,\Pi - \mathbf{grad}\,p \quad (32)$$

where Π is generally the body force potential (here it represents the gravitational force potential), and p is the pressure. For the sake of simplicity, equivalent values will be introduced as follows:

$$\frac{d\vec{\mathbf{U}}}{dt} \equiv \vec{\mathbf{a}};\ \ \mathbf{grad}\,\Pi \equiv \vec{\mathbf{b}};\ \mathbf{grad}\,p \equiv \vec{\mathbf{c}}, \quad (33a)$$

hence, MomCE is:

$$\rho\,\vec{\mathbf{a}} = -\rho\,\vec{\mathbf{b}} - \vec{\mathbf{c}}. \quad (33b)$$

The components of substantial acceleration according to formulas (22–25) will be as follows:

$$a_{x^{(1)}} = a^{(1)}\sqrt{\tilde{g}_{11}} = \frac{\left|\frac{\partial f}{\partial x^{(1)}}\right|}{\frac{\partial f}{\partial x^{(1)}}}\left(-\frac{\left(U_{x^{(2)}}\right)^2}{f} + \frac{\left(U_{x^{(3)}}\right)^2\frac{\partial^2 f}{\partial x^{(3)^2}}}{1+\left(\frac{\partial f}{\partial x^{(3)}}\right)^2}\right) \quad (34)$$

$$a_{x^{(2)}} = a^{(2)}\sqrt{\tilde{g}_{22}} = \frac{U_{x^{(3)}}}{f\sqrt{1+\left(\frac{\partial f}{\partial x^{(3)}}\right)^2}}\frac{\partial}{\partial x^{(3)}}\left(f\,U_{x^{(2)}}\right) \quad (35)$$

$$a_{x^{(3)}} = a^{(3)}\sqrt{\tilde{g}_{33}} = \frac{U_{x^{(3)}}}{\sqrt{1+\left(\frac{\partial f}{\partial x^{(3)}}\right)^2}}\left(\frac{\partial U_{x^{(3)}}}{\partial x^{(3)}} - \frac{U_{x^{(3)}}\frac{\partial f}{\partial x^{(3)}}\frac{\partial^2 f}{\partial x^{(3)^2}}}{1+\left(\frac{\partial f}{\partial x^{(3)}}\right)^2}\right). \quad (36)$$

The gravitational force potential takes the following form in the presented case:

$$\Pi = \Pi\left(x^{(1)}, x^{(3)}\right) = g\left(x^{(3)}\cos\alpha - r\,\sin\alpha\right) \quad (37)$$

where: α is the angle between rotation axis and axis of gravitational force $(\alpha = -135°)$, r is the radius $\left(r = f\left(x^{(1)}, x^{(3)}\right)\right)$ and g is the gravitational acceleration.

Then, the gradient components of this potential, using formulas (19) and (20), will take the following form:

$$b_{x^{(1)}} = b^{(1)}\sqrt{\tilde{g}_{11}} = \frac{\left|\frac{\partial f}{\partial x^{(1)}}\right|}{\frac{\partial f}{\partial x^{(1)}}}\left(\frac{1+\left(\frac{\partial f}{\partial x^{(3)}}\right)^2}{\frac{\partial f}{\partial x^{(1)}}}\frac{\partial \Pi}{\partial x^{(1)}} - \frac{\partial f}{\partial x^{(3)}}\frac{\partial \Pi}{\partial x^{(3)}}\right) \quad (38)$$

$$b_{x^{(2)}} = b^{(2)}\sqrt{\tilde{g}_{22}} = 0 \quad (39)$$

$$b_{x^{(3)}} = b^{(3)}\sqrt{\tilde{g}_{33}} = \sqrt{1+\left(\frac{\partial f}{\partial x^{(3)}}\right)^2}\left(-\frac{\frac{\partial f}{\partial x^{(3)}}}{\frac{\partial f}{\partial x^{(1)}}}\frac{\partial \Pi}{\partial x^{(1)}} + \frac{\partial \Pi}{\partial x^{(3)}}\right). \quad (40)$$

Similarly, the components of the pressure gradient $\mathrm{p}\left(x^{(1)}, x^{(3)}\right)$ take the following form:

$$c_{x^{(1)}} = c^{(1)}\sqrt{\tilde{g}_{11}} = \\ = \frac{\left|\frac{\partial f}{\partial x^{(1)}}\right|}{\frac{\partial f}{\partial x^{(1)}}}\left(\frac{1+\left(\frac{\partial f}{\partial x^{(3)}}\right)^2}{\frac{\partial f}{\partial x^{(1)}}}\frac{\partial p}{\partial x^{(1)}} - \frac{\partial f}{\partial x^{(3)}}\frac{\partial p}{\partial x^{(3)}}\right) \tag{41}$$

$$c_{x^{(2)}} = c^{(2)}\sqrt{\tilde{g}_{22}} = 0 \tag{42}$$

$$c_{x^{(3)}} = c^{(3)}\sqrt{\tilde{g}_{33}} = \\ = \sqrt{1+\left(\frac{\partial f}{\partial x^{(3)}}\right)^2}\left(-\frac{\frac{\partial f}{\partial x^{(3)}}}{\frac{\partial f}{\partial x^{(1)}}}\frac{\partial p}{\partial x^{(1)}} + \frac{\partial p}{\partial x^{(3)}}\right). \tag{43}$$

Taking account of (32) and (33), the MomCE in three directions of the curvilinear coordinate system can be written as follows:

$$\rho\left(-\frac{\left(U_{x^{(2)}}\right)^2}{f} + \frac{\left(U_{x^{(3)}}\right)^2\frac{\partial^2 f}{\partial x^{(3)2}}}{1+\left(\frac{\partial f}{\partial x^{(3)}}\right)^2}\right) = \\ = -\frac{1+\left(\frac{\partial f}{\partial x^{(3)}}\right)^2}{\frac{\partial f}{\partial x^{(1)}}}\left(\rho\frac{\partial \Pi}{\partial x^{(1)}} + \frac{\partial p}{\partial x^{(1)}}\right) + \frac{\partial f}{\partial x^{(3)}}\left(\rho\frac{\partial \Pi}{\partial x^{(3)}} + \frac{\partial p}{\partial x^{(3)}}\right) \tag{44}$$

$$\rho\frac{U_{x^{(3)}}}{f\sqrt{1+\left(\frac{\partial f}{\partial x^{(3)}}\right)^2}}\frac{\partial}{\partial x^{(3)}}\left(f\,U_{x^{(2)}}\right) = 0 \tag{45}$$

$$\rho\frac{U_{x^{(3)}}}{\sqrt{1+\left(\frac{\partial f}{\partial x^{(3)}}\right)^2}}\left(\frac{\partial U_{x^{(3)}}}{\partial x^{(3)}} - \frac{U_{x^{(3)}}\frac{\partial f}{\partial x^{(3)}}\frac{\partial^2 f}{\partial x^{(3)2}}}{1+\left(\frac{\partial f}{\partial x^{(3)}}\right)^2}\right) = \\ = -\rho\sqrt{1+\left(\frac{\partial f}{\partial x^{(3)}}\right)^2}\left(-\frac{\frac{\partial f}{\partial x^{(3)}}}{\frac{\partial f}{\partial x^{(1)}}}\frac{\partial \Pi}{\partial x^{(1)}} + \frac{\partial \Pi}{\partial x^{(3)}}\right) - \\ - \sqrt{1+\left(\frac{\partial f}{\partial x^{(3)}}\right)^2}\left(-\frac{\frac{\partial f}{\partial x^{(3)}}}{\frac{\partial f}{\partial x^{(1)}}}\frac{\partial p}{\partial x^{(1)}} + \frac{\partial p}{\partial x^{(3)}}\right). \tag{46}$$

2.4. Energy conservation equation. Transport of energy in a rotating machine between two points takes place by means of four energy components: 1) kinetic one, 2) pressure, 3) potential and 4) internal energy (if the lack of dissipation is assumed, then the internal energy change is zero). Therefore, the energy conservation equation (ECE) between two points (with the start and end times of t_0 and t, respectively), takes the following form:

$$\left[\frac{1}{2}\left(\left(U_{x^{(3)}}\right)^2 + \left(U_{x^{(2)}}\right)^2\right) + \frac{p}{\rho} + \Pi + e\right]_t - \\ - \left[\frac{1}{2}\left(\left(U_{x^{(3)}}\right)^2 + \left(U_{x^{(2)}}\right)^2\right) + \frac{p}{\rho} + \Pi + e\right]_{t_0} = l \tag{47}$$

where e is the specific internal energy, and l is the specific work added (pump) or removed (turbine) to/from the flow written as follows (it is the so-called Euler's hydraulic machines equation):

$$l = \left[U_{x^{(2)}}U_{rot}\right]_t - \left[U_{x^{(2)}}U_{rot}\right]_{t_0} \tag{48}$$

where U_{rot} is the circumferential (blade) velocity, which is given in the following form:

$$U_{rot} = \omega\, f\left(x^{(1)}, x^{(3)}\right) = \frac{\pi\, n\, f\left(x^{(1)}, x^{(3)}\right)}{30} \tag{49}$$

where ω is the angular velocity [rad/s], and n is the rotational speed [rpm]. In the case of irrotational blades (e.g. guide vanes) $U_{rot} = 0$.

Taking account of formulas (47) and (48), equation of total energy at any point of the streamline can be written in the following form:

$$\frac{1}{2}\left(\left(U_{x^{(3)}}\right)^2 + \left(U_{x^{(2)}}\right)^2\right) - \\ - U_{x^{(2)}}U_{rot} + \frac{p}{\rho} + \Pi + e = e_{tot}\left(x^{(1)}\right) \tag{50}$$

where $e_{tot}\left(x^{(1)}\right)$ is the total energy at inlet to the blade channel (boundary condition for ECE).

Since ECE is a quadratic equation with respect to tangential velocity $U_{x^{(2)}}$, it is possible that in some cases of an ill-posed problem there can be obtained no real solution for this equation due to the negative discriminant Δ:

$$U_{x^{(2)}} = U_{rot} \mp \sqrt{\Delta}\,. \tag{51}$$

It may occur when e.g. the blockage factor or/and blade loading at the inlet are too high. In such a case, the boundary conditions must be modified. If it is difficult to find the proper boundary conditions, this may indicate that the meridional shape of blade is inappropriate for such boundary conditions. It has to be added here that the positive sign in equation (51) is never encountered in hydraulic turbines. The circumferential velocity U_{rot} of the runner is always larger than tangential velocity $U_{x^{(2)}}$ of flow in velocity triangles.

3. Blade shape generation

The method of characteristics was used to solve conservation equations because of the hyperbolic type of the set of equations. It consists of: 1) differentiated ECE with respect to $x^{(3)}$,

2) MomCE in $x^{(1)}$ direction, and the total differentials for 3) pressure dp and 4) tangential velocity $dU_{x^{(2)}}$. It has to be stressed that MassCE is implicitly included. Therefore, the set of equations can be written as follows:

$$\begin{bmatrix} 0 & 1 & 0 & \rho\left(U_{x^{(2)}} - U_{rot}\right) \\ -\dfrac{1+\left(\frac{\partial f}{\partial x^{(3)}}\right)^2}{\frac{\partial f}{\partial x^{(1)}}} & \dfrac{\partial f}{\partial x^{(3)}} & 0 & 0 \\ dx^{(1)} & dx^{(3)} & 0 & 0 \\ 0 & 0 & dx^{(1)} & dx^{(3)} \end{bmatrix} \begin{bmatrix} \frac{\partial p}{\partial x^{(1)}} \\ \frac{\partial p}{\partial x^{(3)}} \\ \frac{\partial U_{x^{(2)}}}{\partial x^{(1)}} \\ \frac{\partial U_{x^{(2)}}}{\partial x^{(3)}} \end{bmatrix} = \tag{52}$$

$$= \begin{bmatrix} \rho\left(-U_{x^{(3)}}\frac{\partial U_{x^{(3)}}}{\partial x^{(3)}} - \frac{\partial \Pi}{\partial x^{(3)}} + U_{x^{(2)}}\frac{\partial U_{rot}}{\partial x^{(3)}}\right) \\ \rho\left(-\frac{\left(U_{x^{(2)}}\right)^2}{f} + \frac{\left(U_{x^{(3)}}\right)^2 \frac{\partial^2 f}{\partial x^{(3)2}}}{1+\left(\frac{\partial f}{\partial x^{(3)}}\right)^2} + \frac{1+\left(\frac{\partial f}{\partial x^{(3)}}\right)^2}{\frac{\partial f}{\partial x^{(1)}}}\frac{\partial \Pi}{\partial x^{(1)}} - \frac{\partial f}{\partial x^{(3)}}\frac{\partial \Pi}{\partial x^{(3)}}\right) \\ dp \\ dU_{x^{(2)}} \end{bmatrix}.$$

The main determinant takes the following form:

$$det = \rho\, dx^{(1)}\left(\frac{\partial f}{\partial x^{(3)}}dx^{(1)} + \right. \\ \left. + \frac{1+\left(\frac{\partial f}{\partial x^{(3)}}\right)^2}{\frac{\partial f}{\partial x^{(1)}}}dx^{(3)}\right)\left(U_{x^{(2)}} - U_{rot}\right). \tag{53}$$

By equating this expression to zero, the following characteristics can be obtained:

- 1st family of characteristics (the family of streamlines along which the $x^{(1)}$ coordinate is constant):

$$dx^{(1)} = 0 \rightarrow x^{(1)} = const\,, \tag{54}$$

- 2nd family of characteristics (the family of orthogonal lines to streamlines):

$$\frac{dx^{(3)}}{dx^{(1)}} = -\frac{\frac{\partial f}{\partial x^{(1)}}\frac{\partial f}{\partial x^{(3)}}}{1+\left(\frac{\partial f}{\partial x^{(3)}}\right)^2}\,, \tag{55}$$

- 3rd family of characteristics (the line of singularity – in such a case, the profile turns back, which is practically not encountered in hydraulic machines):

$$U_{x^{(2)}} = U_{rot}\,. \tag{56}$$

When solving the set of equations (52) with respect to the first unknown, an equation along the second family of characteristics is obtained, which allows for solution of the pressure field (further on, it also allows for calculating the velocity field) inside the blade area:

$$\frac{dp}{dx^{(1)}} = \frac{\rho\frac{\partial f}{\partial x^{(1)}}}{1+\left(\frac{\partial f}{\partial x^{(3)}}\right)^2}\left(\frac{\left(U_{x^{(2)}}\right)^2}{f} - \frac{\left(U_{x^{(3)}}\right)^2\frac{\partial^2 f}{\partial x^{(3)2}}}{1+\left(\frac{\partial f}{\partial x^{(3)}}\right)^2} - \right. \\ \left. - \frac{1+\left(\frac{\partial f}{\partial x^{(3)}}\right)^2}{\frac{\partial f}{\partial x^{(1)}}}\frac{\partial \Pi}{\partial x^{(1)}} + \frac{\partial f}{\partial x^{(3)}}\frac{\partial \Pi}{\partial x^{(3)}}\right). \tag{57}$$

Skeleton (three-dimensional blade surface) of the guide vane or/and runner blade is derived using the equation of the pathline of a fluid element. In absolute velocity formulation, it is given in Cartesian and curvilinear systems, respectively, as follows:

$$\frac{dx^{(2)}}{U^{(2)}-\omega} = \frac{dx^{(3)}}{U^{(3)}} \tag{58a}$$

$$\frac{dx^{(2)}}{U_{x^{(2)}}-U_{rot}} = \frac{\sqrt{1+\left(\frac{\partial f}{\partial x^{(3)}}\right)^2}}{f}\frac{dx^{(3)}}{U_{x^{(3)}}}\,. \tag{58b}$$

In the case of irrotational blades $\omega = 0$.

4. Application of the method and boundary conditions

The presented model was applied to design the guide vane and runner blades for the low-head ($H = 1.5$ m) two-adjustable Kaplan turbine model characterized by a fairly high specific speed n_{sq} (1), larger than 230, with runner diameter $D = Ø300$ mm. Figure 2 shows the meridional shape used for the calculations and its main dimensions. It should be emphasized that the meridional shape adopted for the calculations was not subject to prior optimization (this is not the subject of this paper), therefore, the results obtained should not be considered as optimized from the efficiency point of view.

The used method of characterization requires setting boundary conditions at one of the limitations (hub or shroud line) of the meridional blade shape. In the case of guide vane design,

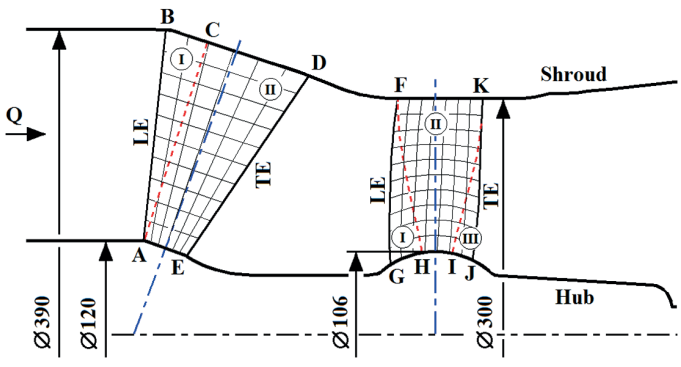

Fig. 2. Schematic meridional view of the low-head Kaplan hydraulic turbine model

some of the orthogonal characteristics to streamlines start at the inlet and cover a region denoted as I (limited by lines ABC) – Fig. 2. The other orthogonal characteristics start at one of the limitations (here: line CD that is the shroud). These characteristics cover the rest of a blade region denoted as II (limited by lines ACDE). Similarly, in the case of runner blade design some of the characteristics start at the inlet and cover region I (limited by curves FGH). The other characteristics start at one of limitations (curve HJ), where the characteristics cover the rest of the blade, i.e. region II (limited by curves FHJK). However, if a zeroth swirl (velocity torque) condition is applied at the outlet $\left(fU_{x^{(2)}} = 0 \rightarrow U_{x^{(2)}} = 0\right)$, then a region denoted as III can be obtained (limited by curves IJK). Region II is then reduced to the one limited by curves FHIK (the characteristics start at the HI curve). Figure 2 shows the orthogonal characteristics (dashed lines) separating the abovementioned regions.

4.1. Guide vane design. Generally, the guide vanes should shut off the flow, which means that they have to be tightly closed (this is not the case when designing a Kaplan turbine runner). In the case of small hydraulic turbines, the guide vane wheel is often the only device that shuts off the water flow. The boundary conditions must take account of this requirement. This is a constraint that significantly limits the guide vane design considerations using the inverse problem. Such a case can be achieved using homogeneous radial inflow (radially uniformly distributed boundary conditions and streamlines) for circumferentially distributed guide vanes (e.g. in a spiral casing of a Francis turbine). In the case of an axial turbine, this is practically unrealizable, so the guide vane should be then modified after the design process. In the presented case, the boundary conditions were adopted in such a way so as to cause (ensure) the minimum necessary interference in guide vane shape achieved using the inverse problem design.

In order to increase outlet velocity in the guide vane, aimed at increasing specific speed n_{sq}, the maximum blade thickness was moved from the initial part of the guide vane towards its center, which was supposed to provide a significant change in water flow direction through the guide vanes. This caused significant increasing of the blade mean line camber. As it has been supposed, on the one hand, inflow with lower incidence was achieved (generally, at the design point the inflow should be free of incidence). On the other hand, this provided a significant swirl to the water flow (at the runner inlet). As a result, large values of optimum opening blade angles (from its physical closure) were obtained (about 60° to 70°). Due to the above-mentioned reasons, the equation determining ϑ thickness was introduced in the following form [29]:

$$\vartheta\left(x^{(1)}, x^{(3)}\right) = t_1 \, \overline{x^{(3)}}^{\,t_2} \left(1 - \overline{x^{(3)}}\right)^{t_3} \left(1 + t_4 \, x^{(1)}\right) \quad (59)$$

where $\overline{x^{(3)}}$ is the non-dimensional axial coordinate $x^{(3)} <0; 1>$, defined as follows:

$$\overline{x^{(3)}}\left(x^{(1)}\right) = \frac{x^{(3)} - x^{(3)}_{inl}\left(x^{(1)}\right)}{x^{(3)}_{out}\left(x^{(1)}\right) - x^{(3)}_{inl}\left(x^{(1)}\right)} \quad (60)$$

and where t_1, t_2, t_3, t_4 are the empirical coefficients, and $x^{(3)}_{inl}\left(x^{(1)}\right)$, $x^{(3)}_{out}\left(x^{(1)}\right)$ are the inlet and outlet axial coordinates of a streamline, respectively. If we add another constraint that maximum thickness ϑ_{max} is located at $\overline{x^{(3)}_{\vartheta_{max}}}$ then some of these coefficient can be calculated in the following form:

$$t_3 = t_2 \left(\frac{1}{\overline{x^{(3)}_{\vartheta_{max}}}} - 1 \right) \quad (61)$$

$$t_1 = \vartheta_{max} \left(\frac{t_2}{t_2 + t_3}\right)^{-t_2} \left(\frac{t_3}{t_2 + t_3}\right)^{-t_3}. \quad (62)$$

According to these two conditions, two parameters remain independent, namely t_2, t_4. Parameter t_2 controls the thickness distribution of the guide vane profile. If required, maximum thickness can be easily shifted in the streamwise direction towards the trailing edge, ensuring the increase of flow rate and thereby increase of specific speed n_{sq}. Parameter t_4 is linearly related to the $x^{(1)}$ coordinate, thus, it controls the thickness change of the profile along the spanwise direction. In the present case t_2, t_4, $\overline{x^{(3)}_{\tau_{max}}}$, and ϑ_{max} were equal to, respectively: 4, –0.2, 0.6 and 0.1.

The other parameters used were as follows: volumetric flow rate $Q = 0.235$ m^3/s, giving meridional velocity $U_{x^{(3)}} = 2.175$ m/s (it was uniformly distributed in the spanwise direction), number of blades 14, no blade loading at the inlet $\left(fU_{x^{(2)}} = 0 \text{ m}^2/\text{s}\right.$ giving the mean blade angle $\alpha = 90°\left.\right)$, and density $\rho = 999.1$ kg/m^3. The number of guide vanes was determined by preceding analysis using CFD calculations. The streamline function consisted of parallel lines. To start the solution on orthogonal characteristics, blade loading at the shroud was assumed using the pressure distribution with respect to relative axial coordinate $\overline{x^{(3)}}$ (Fig. 2 – line BD), as follows:

$$p = p_{inl} - \Delta p \left(\overline{x^{(3)}}\right)^n \quad (63)$$

where $p_{inl} = 100\,000$ Pa is the pressure at the inlet (point B), $\Delta p = 10\,000$ Pa is the drop pressure along line BD and $n = 2.145$ is the coefficient. In the case of an incompressible flow, the level of pressure at the inlet is meaningless because of the linear dependence of pressure in ECE (47).

In order to shape the three-dimensional blade, it was necessary to assume the so-called stacking condition, which means angular coordinate distribution at the leading edge. Since the flow at inlet had no swirl, the lack of circumferential inclination seemed to be the right assumption $\left(x^{(2)}_{inl}\left(x^{(1)}\right) = 0\right)$. Generally, the stacking condition can be assumed anywhere in the meridional plane (including the trailing edge).

As a result of the inverse problem solution, the guide vane is slightly twisted radially. Despite the uniform boundary conditions, a radius change implicitly influences the blade shape, which is included in the momentum conservation equation [30]. The obtained parameters of the guide vane at the outlet were as follows: mean tangential velocity $U_{x^{(2)}} = 4.11$ m/s and mean

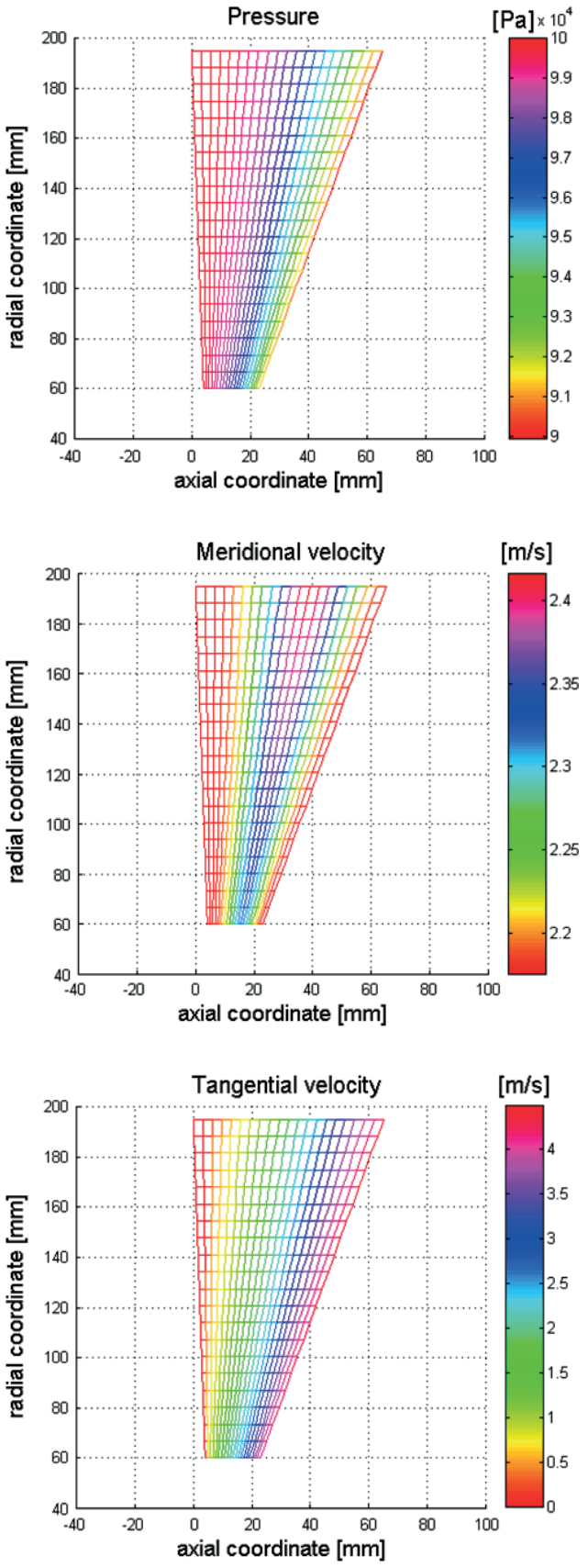

Fig. 4. Contours of the pressure, meridional and tangential velocities in guide vane channel obtained using the inverse problem method (stretched from axi-radial to axial inflow direction)

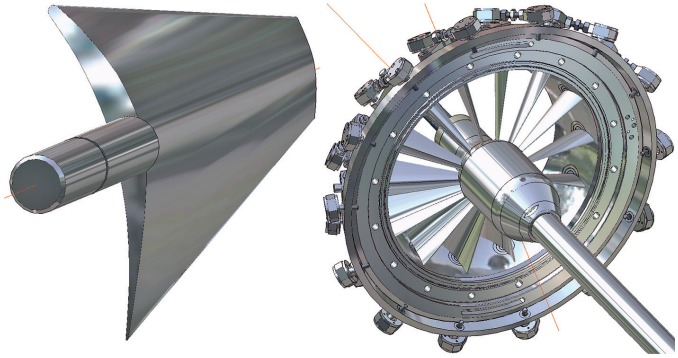

Fig. 3. Views of the single guide vane blade and guide vane wheel of the low-head Kaplan hydraulic turbine model

meridional velocity $U_{x^{(3)}} = 2.17$ m/s. Figure 3 shows the blade of a single guide vane and guide vane wheel of the Kaplan turbine model, and Fig. 4 shows the results of pressure, meridional and tangential velocities obtained using the model presented (visually stretched from axi-radial (see Fig. 2) to axial inflow direction). It should be highlighted that this is an axisymmetric model, therefore the results represent the mean values in circumferential direction.

4.2. Runner blade design. Generally, in order to increase the flow rate (to increase the specific speed), a meridional length of the blade should tend to decrease what causes the increase of torque. The applied meridional shape (Fig. 2) was supposed to ensure a high specific speed larger than $n_{sq} = 230$. The calculated blade and the entire runner wheel are shown in Fig. 5 and in Fig. 6, respectively. At the outlet, no swirl condition was

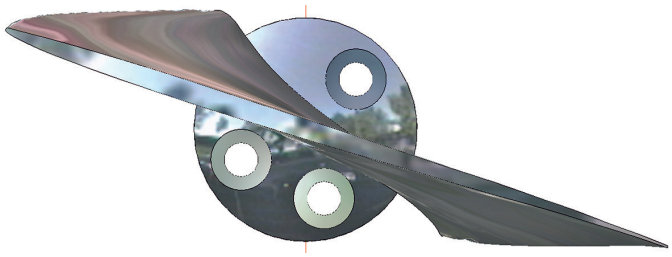

Fig. 5. View of the runner blade of the Kaplan hydraulic turbine model

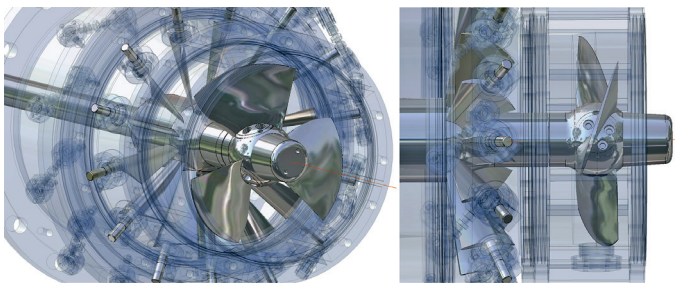

Fig. 6. Views of the runner blade wheel of the Kaplan hydraulic turbine model

set, i.e. tangential velocity was assumed to be $U_{x^{(2)}} = 0$ m/s. This assumption theoretically ensures maximizing the efficiency, which results from Euler's hydraulic turbines equation.

As a blockage factor required for the mass conservation equation (31) the Göttingen 428 profile thickness was used – half the thickness on the suction side and half the thickness on the pressure side was distributed. In the case of a low-head Kaplan turbine runner, the impact of the thickness distribution is relatively small so that it practically has no influence on the flow rate unlike the guide vane, in whose case the thickness distribution plays a key role. Thus, there was no need to introduce a function defining the thickness distribution $\vartheta\left(x^{(1)}, x^{(3)}\right)$.

The number of blades was determined on the basis of analysis of similar low-head Kaplan hydraulic turbine solutions and it was assumed to stand at 3. Such a small number of blades should ensure a large mass flow rate, which characterizes machines with a high specific speed $\left(n_{sq} > 230\right)$, concurrently achieving relatively high efficiency $(>86\%)$.

The other boundary conditions and assumptions for the calculations are presented below. The streamline function was:

$$f\left(x^{(1)}, x^{(3)}\right) = a_1 + (a_2 - a_1)x^{(1)} + \\ + \left(b_1 + (b_2 - b_1)x^{(1)}\right)x^{(3)} + \\ + \left(c_1 + (c_2 - c_1)x^{(1)}\right)\left(x^{(3)}\right)^2 \tag{64}$$

where $a_1 = -2.11527$, $a_2 = 0.1505$, $b_1 = 9.72219$, $b_2 = 0$, $c_1 = -10.897$, and $c_2 = 0$. These coefficients are dependent on the meridional shape of the blade and were obtained in the below-described manner. Firstly, two streamline functions of the same pattern $f = f\left(x^{(3)}\right)$ for hub and shroud lines had to be found separately. In the example considered, this pattern was a quadratic function: $f\left(x^{(3)}\right) = a + bx^{(3)} + c\left(x^{(3)}\right)^2$. These streamline functions were found using the least squares method. Secondly, each coefficient (for hub: a_1, b_1, c_1 and for shroud: a_2, b_2, c_2) was linearly approximated across the spanwise direction with respect to the $x^{(1)}$ coordinate, which changed within the range of $<0; 1>$ Thus, the family of two-dimensional streamlines $f\left(x^{(1)}, x^{(3)}\right)$ was obtained.

The other parameters were assumed as follows: the turbine head $H = 1.5$ m, the rotational speed $n = 810$ rpm, and the density $\rho = 999.1$ kg/m^3. The assumed head strictly influences the Euler's hydraulic machines equation presented in (48) because the specific work l of a turbine may be expressed as follows:

$$l = \eta_h \, g \, H = \eta_h \frac{\Delta p}{\rho} \tag{65}$$

where η_h is the hydraulic efficiency, g is the gravitational acceleration, and Δp is the static pressure difference between inlet (before guide vane wheel) and outlet (behind the draft tube) of the turbine. Thus, it is yet another constraint in ECE that is required to be satisfied.

To start the solution on orthogonal characteristics, blade loading at hub was assumed using the swirl distribution with respect to axial coordinate $x^{(3)}$ (Fig. 2 – curve GHIJ), as follows:

$$f\, U_{x^{(2)}} = a + bx^{(3)} + c\left(x^{(3)}\right)^2 + d\left(x^{(3)}\right)^3 + \\ + e\left(x^{(3)}\right)^4 + f\left(x^{(3)}\right)^5 \tag{66}$$

where $a = 43495$, $b = -478118$, $c = 2099428$, $d = -4602353$, $e = 5036135$, and $f = -2200210$. The presented function allows to calculate the blade loading at hub in region II. However, it is restricted due to the constraints. In regions I and III the flow field is calculated using equation (57) in advance. This means that the swirl at points H and I is known. Therefore, as mentioned, the function is used only in region II (between points H and I) and its shape is strictly dependent on a solution obtained in regions I and III. On this basis, the coefficients using the least squares method were found.

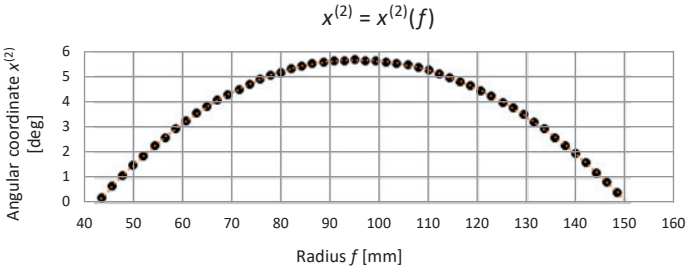

Fig. 7. The stacking condition at the runner inlet used to blade shape calculation

The stacking condition used in skeleton calculations was assumed as a function of angular coordinate $x^{(2)}$ at the runner inlet with respect to radius f (the streamline function at the inlet – see (3)) – Fig. 7. This function was adopted as a 3-degree polynomial, in which the angular coordinate of the lowest and the highest radius is equal to 0°, and additionally in 1/3 and 2/3 of the leading edge length it is equal to 5°:

$$x_{inl}^{(2)} = a + b\, f_{inl}\left(x^{(1)}, x_{inl}^{(3)}\right) + c\, f_{inl}^2\left(x^{(1)}, x_{inl}^{(3)}\right) + \\ + d\, f_{inl}^3\left(x^{(1)}, x_{inl}^{(3)}\right) \tag{67}$$

where $a = -0.23564735$, $b = 7.24726878$, $c = -41.77212782$, and $d = 26.71933415$. Such assumption requires some experience from the designer because it has no mathematical basis while calculating the blade using the inverse problem method. In such a case, the CFD calculations can be indispensable to evaluate influence of the stacking condition on flow parameters.

The obtained mean velocities of the runner blade at the inlet were as follows: tangential velocity $U_{x^{(2)}} = 1.69$ m/s and meridional velocity $U_{x^{(3)}} = 3.55$ m/s. Respectively, at the outlet meridional velocity was $U_{x^{(3)}} = 3.5$ m/s.

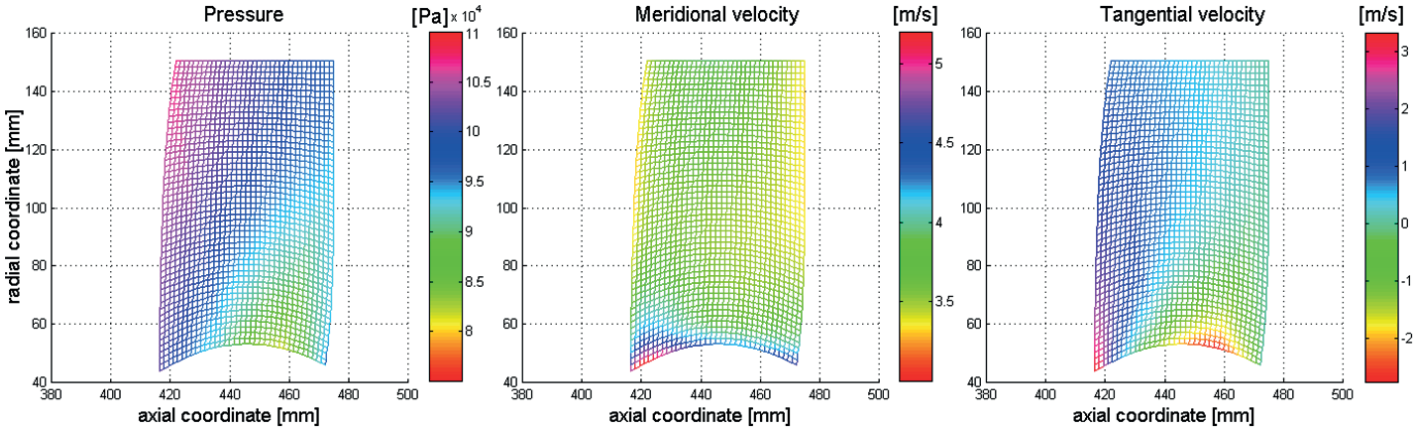

Fig. 8. Contours of the pressure, meridional and tangential velocities in runner blade channel obtained using the inverse problem method

Figure 8 shows the results of pressure, meridional and tangential velocities obtained in the runner blade channel using the model presented. The results indicate a tendency for flow separation on the hub nearby the outlet zone (as mentioned, the meridional shape was not subject to optimization), which should/could be the subject of further blade shape optimization, e.g. using CFD tools.

5. CFD investigations and results

CFD calculations were carried out for the designed flow system, and their computational domain is shown in Fig. 9. The calculations were made for a wide range of changes of the guide vane opening, the runner opening and the rotational speed, in which as it had been supposed the BEP should subsequently appear. Therefore, 4 settings of the runner blades: 14°, 16°, 18°, 20° were used for the calculations, and in each of the mentioned settings the following 5 guide vane settings: 55°, 60°, 65°, 70°, 75° were used, and additionally for each the runner and guide vane settings different rotational speeds: 550, 610, 670, 730, 790, 850, 910 and 970 rpm were assumed (in total, $4\times5\times8 = 160$ computational cases were analyzed). Based on this, the optimal work point has been estimated.

Figure 9 also shows reference cross-sections (inlet and outlet) that were used to define efficiency of the flow system. The efficiency was defined as follows:

$$\eta = \frac{M\omega}{Q\,\rho\,g\,H} \tag{68}$$

where M is the shaft moment $[\mathrm{Nm}]$, ω is the rotational velocity $[\mathrm{rad/s}]$, Q is the volumetric flow rate $[\mathrm{m^3/s}]$, ρ is the density $[\mathrm{kg/m^3}]$, g is the gravitational acceleration $[\mathrm{m/s^2}]$ and H is the head $[\mathrm{m}]$ between the reference cross-sections defined as follows:

$$H = \frac{\Delta p}{\rho\, g} + \frac{V_1^2 - V_2^2}{2\, g} \tag{69}$$

where Δp is the pressure difference between inlet and outlet reference cross-sections (Fig. 9), V_1 is the mean velocity at inlet

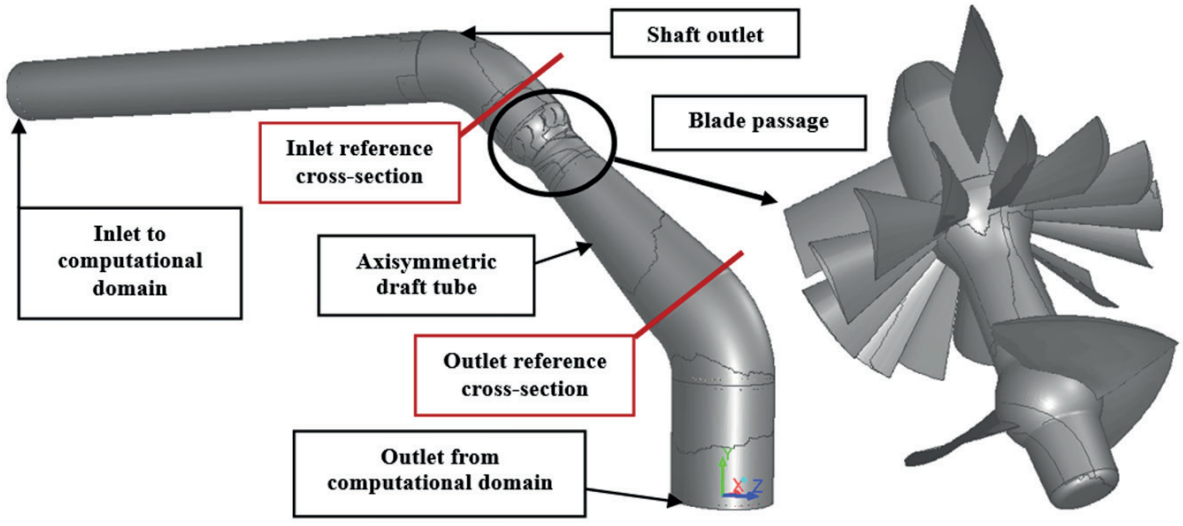

Fig. 9. Views of the computational domain used to CFD calculation and the blades passage

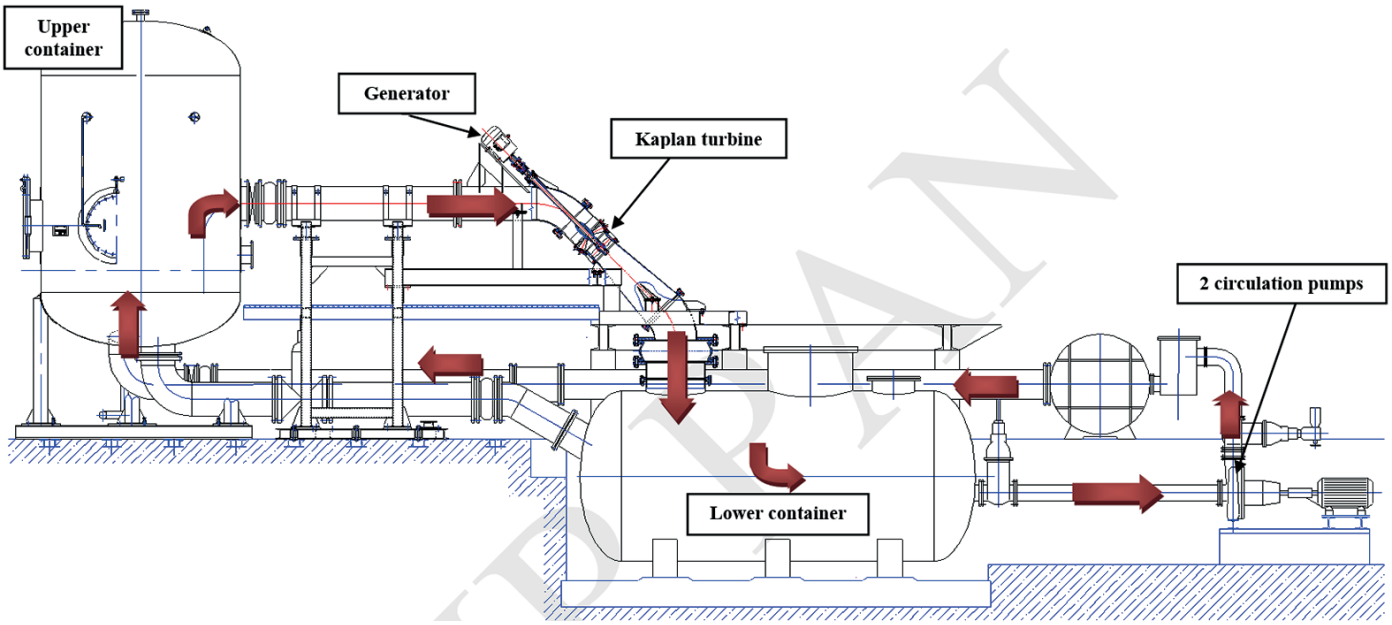

Fig. 10. Schematic of the test stand for hydraulic turbines investigations in IMP PAN with the low-head Kaplan turbine model installed

reference cross-section: $V_1 = Q/A_1$, V_2 is the mean velocity at outlet reference cross-section: $V_2 = Q/A_2$, and A_1, A_2 are the areas of inlet and outlet reference cross-sections, respectively.

Computational mesh was made using two NUMECA programs: AutoGrid5™ and Hexpress™. The number of mesh nodes (entirely hexahedral) was ∼20 million. The mesh was made according to the requirements of the turbulent model *k-ω SST* used for calculations, for which the value of dimensionless distance from the wall Y^+ has to be in range of 1–3. It should be added that the runner tip gap had not been modelled, and as a result, the efficiency was expected not to take account of volumetric losses. The calculations were performed using ANSYS/Fluent™ 15 (second order discretization scheme, steady flow). The boundary conditions applied in the calculations were the following (flow forced by pressure difference): total pressure at inlet to the computational domain: ∼15 500 Pa, and static pressure at outlet from the computational domain: 0 Pa.

As a result of calculations, the following kinematic and flow parameters in the BEP were obtained: the rotational speed $n = 790$ rpm, the volumetric flow rate $Q = 0.194$ m^3/s, turbine efficiency $\eta = 90.1\%$, the guide vane opening angle $\alpha = 61°$, the runner opening $\beta = 15°$, the kinematic specific speed $n_{sq} = \sim 259$ (dynamic: ∼900), the double reduced rotational speed $n_I^I = 194$ rpm $\left(n_I^I = nD/H^{0.5}\right)$, and the double reduced volumetric flow rate $Q_I^I = 1.77$ m^3/s $\left(Q_I^I = Q/\left(D^2H^{0.5}\right)\right)$. The double reduced quantities indicate the rotational speed and the flow rate of a turbine with the runner diameter of 1 m operating under the head of 1 m.

6. Experimental investigations and results

The performance investigations were carried out at the test stand at the Institute of Fluid-Flow Machinery (IMP PAN) in Gdańsk, Poland. Schematic diagrams of the test stand and of the Kaplan hydraulic turbine are presented in Fig. 10 and Fig. 11, respectively. In Fig. 11, the pressure manifolds in reference cross-sections used for pressure difference collection required for efficiency definition (68) were presented. The locations of the reference cross-sections were similar as those used in CFD calculation. The characteristic diameter of the runner was

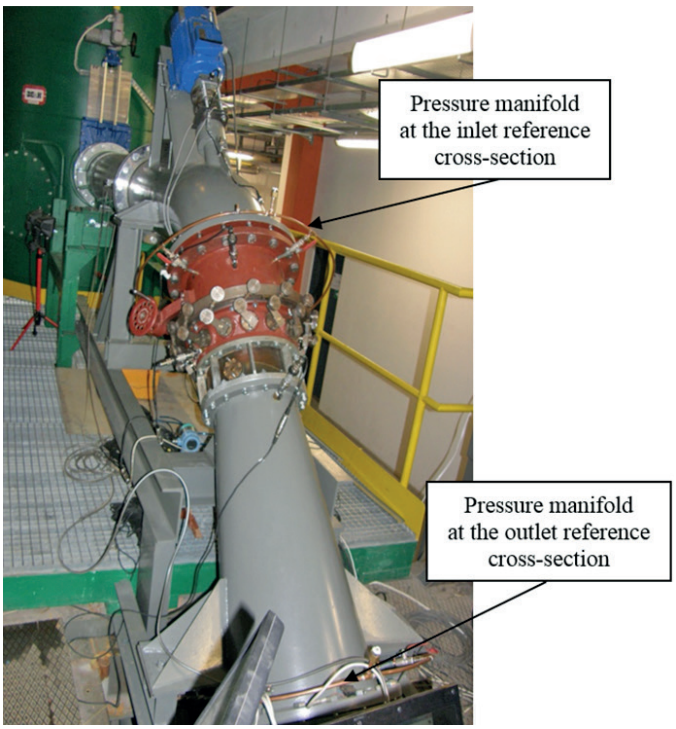

Fig. 11. View of the low-head Kaplan hydraulic turbine model installed at the test stand

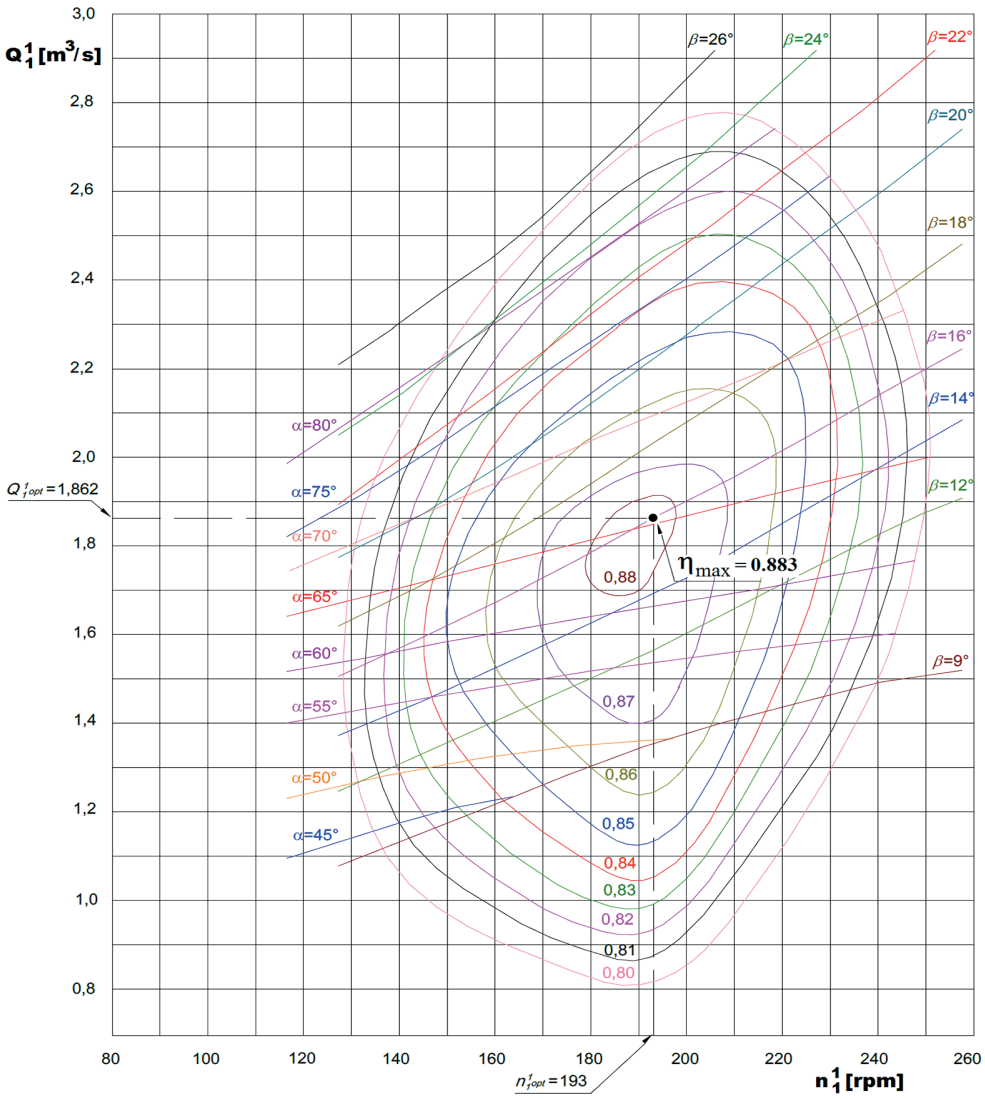

Fig. 12. The shell characteristics of the low-head Kaplan hydraulic turbine model

assumed to be $D = Ø300$ mm. The other dimensions of the flow elements were determined in accordance with this diameter. The straight long intake pipeline was ended with a 45° curved elbow. Behind it, the water flowed directly to the axial blade system of the stationary and adjustable guide vanes, and the runner. The shaft connecting the turbine (up to 5 kW) and generator (via torque transducer) was led upstream outside. The inlet diameter before the guide vanes was Ø390 mm. Behind the runner, an axisymmetric draft tube with an opening angle of 12°, and of the length of more than 3 runner diameters (which is the recommended minimum) was installed. The angle mentioned was established on the basis of numerical experiments, which showed that it should ensure no flow separation at the wall. The correct selection of this angle may significantly improve overall hydro unit operation because, in the case of a low-head turbine, it is a crucial issue for maximizing efficiency due to the optimum energy recovery of static pressure (reduction of outlet loss).

The investigations were carried out at head $H = 1.5$ m for 9 angular settings of the runner blades, namely: 9°, 12°, 14°, 16°, 18°, 20°, 22°, 24° and 26°. The mentioned angular settings are understood as the angles of attack at the top radius. For each runner blade setting, the guide vanes was adjusted every 5°. The range of variation was dependent on the runner blade setting. For setting 9°, the guide vanes were adjusted within the range of 35°–75° from their physical closure, while for 26°, the guide vanes were adjusted from 45° to 80°. At the given guide vanes and runner settings, tests were conducted by changing the rotational speed of the turbine from the smallest to the largest values every ca. 50 rpm (within the range of 400–980 rpm). The rotational speed of turbine was controlled by changing (by means of frequency converters) the rotational speed of circulation pumps. In total, over 800 measuring points were made. As a result of the experimental tests, the so-called shell characteristics were obtained, which is the efficiency diagram related to the double reduced rotational speed n_I^I, and the double reduced volumetric flow rate Q_I^I.

The obtained shell characteristics are shown in Fig. 12. The following performance parameters were achieved in

the BEP: rotational speed $n = 788$ rpm, volumetric flow rate $Q = 0.2053$ m^3/s, turbine efficiency $\eta = 88.3\%$, guide vane angle $\alpha = 65°$, runner opening $\beta = 16°$, kinematic specific speed $n_{sq} = \sim 260$ (1), double reduced rotational speed $n_I^I = 193$ rpm and double reduced volumetric flow rate $Q_I^I = 1.862$ m^3/s.

The efficiency obtained should be objectively regarded as more than good at this scale of a model machine characterized by such a high specific speed, for which obtaining relatively high efficiency is fairly difficult due to the cavitation. It should be stressed that at the optimum point of work it was not observed. The design of the turbine with larger specific speed n_{sq} is a very difficult task due to this phenomenon, which is dangerous for the machine life.

In comparison to CFD calculations, the level of efficiency obtained is lower by about 1.8%, however the runner tip gap had not been modelled, as a result of which numerical efficiency is expectedly overestimated by including volume losses (it is commonly accepted that they are in the range of 1–2%). Therefore, it should be acknowledged that the maximum efficiency obtained in the numerical way was approximated in a satisfactory manner along with the double-reduced parameters and specific speed.

Cavitation is a very dangerous phenomenon occurring in hydraulic machines that can lead to destruction of flow elements (the runner is most exposed to cavitation erosion). Its prediction is a key design issue. Figure 13 shows the calculated local (in grid points) cavitation number σ in the runner (this is the so-called Thoma number), which was defined as follows:

$$\sigma_{i,j} = \frac{p_{i,j} + \frac{1}{2}\rho\, c_{i,j}^2 - p_{vap}}{\frac{1}{2}\rho U_{rot}^2} \tag{70}$$

where i, j are the indices of a local grid point in the streamline and spanwise directions, $p_{i,j}$ and $c_{i,j}$ are the pressure and velocity in a local grid point, respectively, p_{vap} is the vapour pressure, U_{rot} is the maximum blade velocity and ρ is the density.

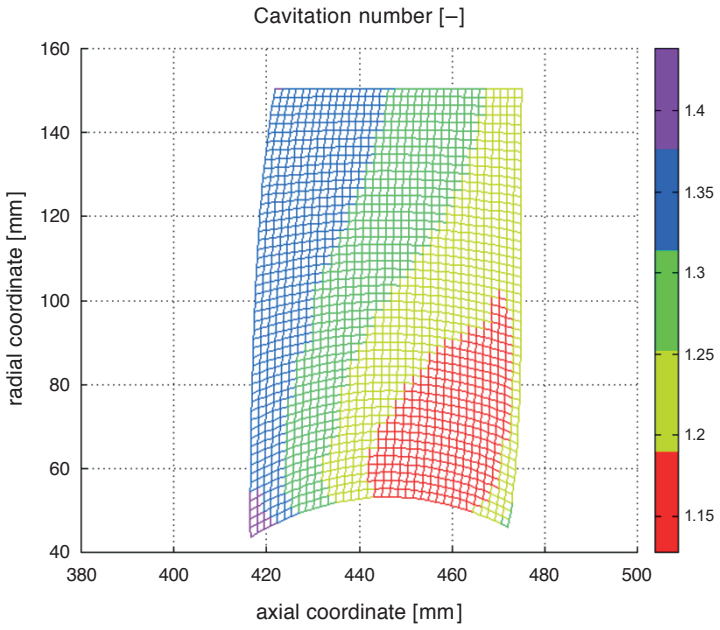

Fig. 13. Cavitation number distribution in the runner

Thoma number determines how the hydraulic turbine runner should be positioned relative to the tailwater level. Experimental investigations indicate that cavitation will not occur if the so-called suction height H_s does not exceed the value defined by inequality [31]:

$$H_s \leq 13.6\frac{p_{bar}}{1000} - \frac{p_{vap}}{10000} - \sigma H \tag{71}$$

where p_{bar} is the barometric pressure [mmHg], and H is the head [m]. Note that the vapor pressure p_{vap} is expressed in [Pa]. For calculated mean value of $\sigma = 1.28$, and $p_{bar} = 760$ mmHg, $p_{vap} = 1704$ Pa, and $H = 1.5$ m, the suction head H_s is ca. 8 m. This means that the runner can be located 8 m above the tailwater level without the occurrence of the cavitation phenomenon (such value is very favorable). As it can be seen (Fig. 13), the largest values occur in the inlet region of the blade due to high velocities. In the outlet region, influence of the zero swirl condition (boundary condition) is clearly visible.

7. Discussion and conclusions

The inverse problem based on the hodograph theory for the low-head Kaplan hydraulic turbine model characterized by high specific speed has been presented. In particular, its principles based on a curvilinear coordinate system have been shown. Such approach significantly simplifies the conservation equations and thus significantly simplifies the way of solving them. The solution of the problem, using the characteristics method, leads to three-dimensional geometry of a blade. The method is derived for zero blade thickness, but concurrently the blockage factor introduced into the mass conservation equation is taken into account, so that it affects the meridional velocity related to mass flow rate.

To validate the method presented herein, the guide vane and runner blade design of the Kaplan hydraulic turbine model was created. As a result, a relatively high-efficiency flow system was obtained (numerically and experimentally confirmed). Adoption of a meridional shape depends to a large extent on rotational specific speed n_{sq} (as a combination of rotational speed, flow rate and head), which in advance predetermines a shape that only can change within a small range. This requires some experience from the designer. In the presented case, the meridional shape was used, which corresponds to a high specific speed low-head Kaplan turbine. The very good efficiency of 88.3% (no cavitation phenomenon was observed in the BEP) obtained for the turbine during experimental research indicates correctness of the formulated design problem (BEP was characterized by a very high specific speed $n_{sq} = \sim 260$).

The usefulness and robustness of the method is strictly limited to the well-posed boundary conditions. The boundary conditions determining blade loading may be implemented by means of swirl or pressure distribution along one of the meridional channel limitations (hub or shroud). This distribution is based on strict assumptions (constraints) at the inlet and outlet

of the blade, resulting from hydraulic turbines theory. It should ensure a small margin of error in setting such a type of boundary condition. Such condition can be optimized e.g. to maximize efficiency. Additionally, well-posed boundary conditions (which means that they exist, are unique and continuous) are key for achieving the solution. If the problem is ill-posed, no real solution can be obtained due to the quadratic dependency of tangential velocity in the energy conservation equation. The blockage factor, which accelerates the flow, also has a large influence on the solution obtained. Generally, the smaller the number of blades, the smaller the influence of a blockage factor that can be observed, so in the case of a runner blade (of a low-head Kaplan turbine) it is insignificant but in the case of a guide vane it is of crucial meaning.

The presented method can be applied to other types of hydraulic machines (Francis turbines, axial and mixed flow pumps). Its usage allows for conducting quick engineering blade design of a rotating machine. Because this is the inverse problem method, the blade is designed for the optimum point of operation (BEP). Then, it seems necessary to check such a solution using commercial CFD software, in order to avoid a large mistake and, additionally, to check the performance at off-design points of operation.

Acknowledgements. This work was supported by the (Polish) National Science Centre (NCN) under grant No. PB 6694/B/T02/2011/40 entitled "*Development of design methodology for low-head axial turbines*". The CFD computations were carried out on PL-Grid infrastructure. *In memoriam*, the author specially wishes to thank Professor Romuald Puzyrewski (1935–2016, R.I.P.) from Gdańsk University of Technology (Poland) with whom he collaborated through many years and who taught him the inverse problem method.

References

[1] C.H. Wu, "A general theory of three-dimensional flow in subsonic and supersonic turbomachines of axial-, radial-, and mixed-flow types", NACA Technical Note 2604, 1952.

[2] C.H. Wu, "A general theory of two- and three-dimensional rotational flow in subsonic and transonic turbomachines", NASA Contractor Report 4496, 1993.

[3] W.R. Hawthorne, C. Wang, C.S. Tan, and J.E. McCune, "Theory of blade design for large deflections – Part 1: two-dimensional cascade", *ASME J. Eng. Gas Turbines Power* 106(2), 346–353 (1984).

[4] C.S. Tan, W.R. Hawthorne, J.E. McCune, and C. Wang, "Theory of blade design for large deflections – Part 2: annular cascades", *ASME J. Eng. Gas Turbines Power* 106(2), 354–365 (1984).

[5] M. Zangeneh, "A compressible three dimensional blade design method for radial and mixed flow turbomachinery blades", *Int. J. Numer. Methods Fluids* 13(5), 599–624 (1991).

[6] M. Zangeneh, "Inverse design of centrifugal compressor vaned diffusers in inlet shear flows", *ASME J. Turbomach.* 118(2), 385–393 (1996).

[7] A. Demeulenaere and R.A. van den Braembussche, "Three-dimensional inverse method for turbomachinery blading design", *ASME J. Turbomach.* 120(2), 247–255 (1996).

[8] L. de Vito, R.A. van den Braembussche, and H. Deconinck, "A novel two-dimensional viscous inverse design method for turbomachinery blading", *ASME J. Turbomach.* 125(2), 310–316 (2003).

[9] A. Goto and M. Zangeneh, "Hydrodynamic design of pump diffuser using inverse design method and CFD", *ASME J. Fluids Engineering* 124(2), 319–328 (2002).

[10] A. Goto, M. Nohmi, T. Sakurai, and Y. Sogawa, "Hydrodynamic design system of for pumps based on 3-D CAD, CFD, and inverse design method", *ASME J. Fluids Engineering* 124(2), 329–335 (2002).

[11] S. Cao, G. Peng, and Z. Yu, "Hydrodynamic design of rotodynamic pump impeller for multiphase pumping by combined approach of inverse design and CFD analysis", *ASME J. Fluids Engineering* 127(2), 330–338 (2005).

[12] G. Peng, "A practical combined computation method of mean through-flow for 3D inverse design of hydraulic turbomachinery blades", *ASME J. Fluids Engineering* 127(6), 1183–1190 (2005).

[13] R.H. Zhang, R. Guo, J.H. Yang, and J.Q. Luo. "Inverse method of centrifugal pump impeller based on proper orthogonal decomposition (POD) method", *Chin. J. Mech. Eng.* 30(4), 1025–1031 (2017).

[14] L. Yeming, X.F. Wang, W. Wang, and F.M. Zhou, "Application of the modified inverse design method in the optimization of the runner blade of a mixed-flow pump", *Chin. J. Mech. Eng.* 31(1), 105–121 (2018).

[15] G. Peng, S. Cao, M. Ishizuka, and S. Hayama, "Design optimization of axial flow hydraulic turbine runner: Part I – an improved Q3D inverse method", *Int. J. for Numerical Methods in Fluids* 39(6), 517–531 (2002).

[16] G. Peng, S. Cao, M. Ishizuka, and S. Hayama, "Design optimization of axial flow hydraulic turbine runner: Part II – multi-object constrained optimization method", *Int. J. for Numerical Methods in Fluids* 39(6), 533–548 (2002).

[17] M. Zangeneh, A. Goto, and T. Takemura, "Suppression of secondary flows in a mixed flow pump impeller by application of 3D inverse design method: Part 1 – design and numerical validation", *ASME J. Turbomach.* 118(3), 536–543 (1996).

[18] K. Daneshkah and M. Zangeneh, "Parametric design of a Francis turbine runner by means of a three-dimensional inverse design method", IOP Conf. Series: *Earth and Environmental Science* 12, 012058 (2010).

[19] H. Okamoto and A. Goto, "Suppression of cavitation in a Francis turbine runner by application of 3D inverse design method*". ASME Joint U.S.-European Fluids Engineering Division Conference*, paper no. 31192, 851–858 (2002).

[20] D. Bonaiuti, M. Zangeneh, R. Aartojarvi, and J. Eriksson, "Parametric design of a waterjet pump by means of inverse design. CFD calculations and experimental analyses", *ASME J. Fluids Engineering*, 132(3), 031104 (2010).

[21] J.E. Borges, "A three-dimensional inverse method for turbomachinery – Part 1: theory", *J. Turbomach.* 112(3), 346–354 (1990).

[22] J. Jiang and T. Dang, "Design method for turbomachine blades with finite thickness by the circulation method", *J. Turbomach.* 119(3), 539–543 (1997).

[23] J.C. Pascoa, A.C. Mendes, and L.M.C. Gato, "A fast iterative inverse method for turbomachinery blade design", *Mech. Res. Commun*. 36(5), 630–637 (2009).

[24] N.P. Kruyt and R.W. Westra, "On the inverse problem of blade design for centrifugal pumps and fans", *Inverse Problems* 30(6), 065003 (2014).

[25] X. Qiu, M. Ji, and T. Dang, "Three-dimensional viscous inverse method for axial blade design", *Inverse Problems Sci. Eng.* 17(8), 1019–1036 (2009).
[26] K. Daneshkhah and W. Ghaly, "An inverse blade design method for subsonic and transonic viscous flow in compressors and turbines", *Inverse Problems Sci. Eng.* 14(3), 211–231 (2006).
[27] https://en.wikipedia.org/wiki/Christoffel_symbols.
[28] R. Puzyrewski, "Podstawy teorii maszyn wirnikowych w ujęciu jednowymiarowym (Basic Theory of Rotating Machinery in Terms of 1D Model)", the Ossolinskis Publisher, Wroclaw--Warszawa-Krakow, ISBN 83–04–03829–3, 1992, [in Polish].
[29] R. Puzyrewski and Z. Krzemianowski, "Two concepts of guide vane profile design for a low head hydraulic turbine", *Journal of Mechanics Engineering and Automation* 5(4), 201–209 (2015).
[30] R. Puzyrewski and Z. Krzemianowski, "2D model of guide vane for low head hydraulic turbine. Analytical and numerical solution of inverse problem", *Journal of Mechanics Engineering and Automation* 4(3), 195–202 (2014).
[31] W. Krzyżanowski, "Turbiny wodne. Konstrukcja i zasady regulacji (Hydraulic turbines. Construction and regulation)", WNT Publisher, Warsaw, Poland, 1971, [in Polish].

Appendix

Below in Table A1, according to the assumptions of the presented model, the Christoffel symbols of the second kind $\Gamma_{i,j}^{k}$ (14) used in the conservation equations are presented.

Table A1.
The Christoffel symbols of the Second Kind used in the presented model

$\Gamma_{1,1}^{1} = \vec{e}^{1} \circ \frac{\partial^2 \vec{r}}{\partial x^{(1)^2}} = \frac{\frac{\partial^2 f}{\partial x^{(1)^2}}}{\frac{\partial f}{\partial x^{(1)}}}$	$\Gamma_{1,1}^{2} = \vec{e}^{2} \circ \frac{\partial^2 \vec{r}}{\partial x^{(1)^2}} = 0$	$\Gamma_{1,1}^{3} = \vec{e}^{3} \circ \frac{\partial^2 \vec{r}}{\partial x^{(1)^2}} = 0$
$\Gamma_{1,2}^{1} = \vec{e}^{1} \circ \frac{\partial^2 \vec{r}}{\partial x^{(2)} \partial x^{(1)}} = 0$	$\Gamma_{1,2}^{2} = \vec{e}^{2} \circ \frac{\partial^2 \vec{r}}{\partial x^{(2)} \partial x^{(1)}} = \frac{\frac{\partial f}{\partial x^{(3)}}}{f}$	$\Gamma_{1,2}^{3} = \vec{e}^{3} \circ \frac{\partial^2 \vec{r}}{\partial x^{(2)} \partial x^{(1)}} = 0$
$\Gamma_{1,3}^{1} = \vec{e}^{1} \circ \frac{\partial^2 \vec{r}}{\partial x^{(3)} \partial x^{(1)}} = \frac{\frac{\partial^2 f}{\partial x^{(3)} \partial x^{(1)}}}{\frac{\partial f}{\partial x^{(1)}}}$	$\Gamma_{1,3}^{2} = \vec{e}^{2} \circ \frac{\partial^2 \vec{r}}{\partial x^{(3)} \partial x^{(1)}} = 0$	$\Gamma_{1,3}^{3} = \vec{e}^{3} \circ \frac{\partial^2 \vec{r}}{\partial x^{(3)} \partial x^{(1)}} = 0$
$\Gamma_{2,1}^{1} = \vec{e}^{1} \circ \frac{\partial^2 \vec{r}}{\partial x^{(1)} \partial x^{(2)}} = 0$	$\Gamma_{2,1}^{2} = \vec{e}^{2} \circ \frac{\partial^2 \vec{r}}{\partial x^{(1)} \partial x^{(2)}} = \frac{\frac{\partial f}{\partial x^{(3)}}}{f}$	$\Gamma_{2,1}^{3} = \vec{e}^{3} \circ \frac{\partial^2 \vec{r}}{\partial x^{(1)} \partial x^{(2)}} = 0$
$\Gamma_{2,2}^{1} = \vec{e}^{1} \circ \frac{\partial^2 \vec{r}}{\partial x^{(2)^2}} = -\frac{f}{\frac{\partial f}{\partial x^{(1)}}}$	$\Gamma_{2,2}^{2} = \vec{e}^{2} \circ \frac{\partial^2 \vec{r}}{\partial x^{(2)^2}} = 0$	$\Gamma_{2,2}^{3} = \vec{e}^{3} \circ \frac{\partial^2 \vec{r}}{\partial x^{(2)^2}} = 0$
$\Gamma_{2,3}^{1} = \vec{e}^{1} \circ \frac{\partial^2 \vec{r}}{\partial x^{(3)} \partial x^{(2)}} = 0$	$\Gamma_{2,3}^{2} = \vec{e}^{2} \circ \frac{\partial^2 \vec{r}}{\partial x^{(3)} \partial x^{(2)}} = \frac{\frac{\partial f}{\partial x^{(3)}}}{f}$	$\Gamma_{2,3}^{3} = \vec{e}^{3} \circ \frac{\partial^2 \vec{r}}{\partial x^{(3)} \partial x^{(2)}} = 0$
$\Gamma_{3,1}^{1} = \vec{e}^{1} \circ \frac{\partial^2 \vec{r}}{\partial x^{(1)} \partial x^{(3)}} = \frac{\frac{\partial^2 f}{\partial x^{(1)} \partial x^{(3)}}}{\frac{\partial f}{\partial x^{(1)}}}$	$\Gamma_{3,1}^{2} = \vec{e}^{2} \circ \frac{\partial^2 \vec{r}}{\partial x^{(1)} \partial x^{(3)}} = 0$	$\Gamma_{3,1}^{3} = \vec{e}^{3} \circ \frac{\partial^2 \vec{r}}{\partial x^{(1)} \partial x^{(3)}} = 0$
$\Gamma_{3,2}^{1} = \vec{e}^{1} \circ \frac{\partial^2 \vec{r}}{\partial x^{(2)} \partial x^{(3)}} = 0$	$\Gamma_{3,2}^{2} = \vec{e}^{2} \circ \frac{\partial^2 \vec{r}}{\partial x^{(2)} \partial x^{(3)}} = \frac{\frac{\partial f}{\partial x^{(3)}}}{f}$	$\Gamma_{3,2}^{3} = \vec{e}^{3} \circ \frac{\partial^2 \vec{r}}{\partial x^{(2)} \partial x^{(3)}} = 0$
$\Gamma_{3,3}^{1} = \vec{e}^{1} \circ \frac{\partial^2 \vec{r}}{\partial x^{(3)^2}} = \frac{\frac{\partial^2 f}{\partial x^{(3)^2}}}{\frac{\partial f}{\partial x^{(1)}}}$	$\Gamma_{3,3}^{2} = \vec{e}^{2} \circ \frac{\partial^2 \vec{r}}{\partial x^{(3)^2}} = 0$	$\Gamma_{3,3}^{3} = \vec{e}^{3} \circ \frac{\partial^2 \vec{r}}{\partial x^{(3)^2}} = 0$